Discrete Terahertz tomography: a simulation study

Jana Christopher, Lars-Paul Lumbeeck, Pavel Paramonov, Jan De Beenhouwer, Jan Sijbers[1]

[1]imec-Visionlab, University of Antwerp, Universiteitsplein 1, B-2610, Antwerp, Belgium,
E-mail: janachristopher97@gmail.com, lars-paul.lumbeeck@uantwerpen.be, pavel.paramonov@uantwerpen.be,
jan.debeenhouwer@uantwerpen.be, jan.sijbers@uantwerpen.be

Abstract

As Terahertz (THz) technology becomes more prominent in the imaging industry, there is a rising need for improved reconstruction techniques for THz tomographic imaging. Conventional reconstruction techniques yield artifacts for limited data problems, hindering further analysis of the reconstruction. In this paper, we explore a discrete reconstruction algorithm for Terahertz tomography, which exploits prior knowledge on the gray levels in the imaging data of the object to obtain high quality reconstructions. Simulations show that, compared to THz-SIRT reconstruction, the discrete THz algorithm (THz-DART) generates more accurate reconstructions, especially when only a small number of projections or projections acquired within a limited angular range are available.

Keywords: Terahertz imaging, computed tomography, discrete reconstruction, DART

1 Introduction

THz tomography is a research field of increasing interest due to the beam's unique interactions with matter. It is a non-ionizing, non-invasive and non-destructive imaging technique. Applications cover a wide range of fields, including quality control in various industries [1], security screening [2], the study of biological materials [3], and art inspection [4]. Computed tomography (CT) reconstruction methods applied to THz data are often based on the X-Ray Radon transform [5]. However, in contrast to X-ray CT systems, in THz CT systems, the generated beam has a non-zero thickness, resulting in an intrinsic projection blur [6]. Recently, simulation techniques for accurate THz beam simulation were proposed [7, 8], as well as a THz reconstruction algorithm that incorporates the THz beam shape into the Radon Transform [9]. Iteratively approximating the inverse of this modified transform showed improved reconstruction quality and convergence speed compared to conventional filtered backprojection.
In tomographic experiments, limited data problems are common: having few projection directions or a limited angular range for instance to reduce the scan time or when acquiring projection from certain angles is physically impossible due to limited access of the object. In these limited data problems, Radon Transform based methods are known to lead to severe reconstruction artefacts. Fortunately, exploiting prior knowledge of the object can alleviate such artefacts to a certain degree. For objects consisting of a limited number of materials, prior knowledge on the gray levels in the reconstruction can be exploited, for example by using a discrete reconstruction algorithm (DART) [10]. In this paper, we describe a DART-based reconstruction algorithm for Terahertz tomography and show, by means of simulation experiments, that substantially improved images can be obtained, specifically in case of limited angle THz imaging problems.

2 Methods

The THz beam 2D intensity profile can be approximated with a Gaussian distribution:

$$I^{2D}(x,y) = I_0\sqrt{\frac{\pi}{2}}\frac{\omega_0^2}{\omega(y)}e^{-\frac{2x^2}{\omega^2(y)}} \tag{1}$$

with $\omega(y) = \omega_0\sqrt{1+(\frac{z}{z_R})^2}$ the width function of the beam, ω_0 the beam waist, and z_R the Rayleigh range $z_R = \frac{\pi\omega_0^2}{\lambda}$. To incorporate the beam shape in the THz Radon transform, the image $f(x,y)$ is convolved with the Gaussian beam intensity [6, 9]:

$$p_\theta(\rho) = \iint f * I_\theta^{2D}(x,y)\delta(\rho - x\cos\theta - y\sin\theta)\,dxdy \tag{2}$$

The reconstruction is represented on a pixel grid of width w and height h, with the total number of pixels: $n = wh$. Measurements are taken as a set of projections from different angles. The total number of measurements is denoted by: $m = kd$, with d the number of projection angles and k the number of equally spaced detector cells. The forward projection can be described using a projection matrix $\mathbf{W}$, where the element w_{ij} contains the weight of the contribution of the pixel i to the measurement j. In a discrete representation, the X-ray forward projection is described by:

$$\mathbf{Wx} = \mathbf{p} \tag{3}$$

https://doi.org/10.58286/26608

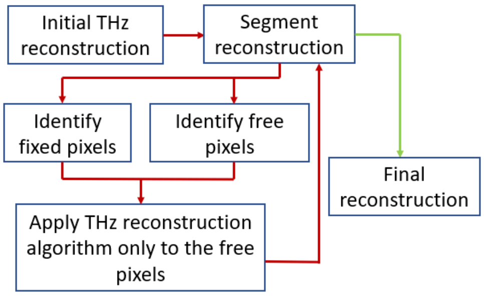

Figure 1: Flowchart of THz-DART algorithm.

where $\mathbf{W} \in \mathbb{R}^{m\times n}$, $\mathbf{x} \in \mathbb{R}^n$ contains the pixel values of the reconstruction and $\mathbf{p} \in \mathbb{R}^m$ is the set of measured projections or the sinogram. By incorporating the Gaussian beam shape, the THz forward projection can be defined by the set of linear equations [9]:

$$\mathbf{CWHx} = \mathbf{p} \tag{4}$$

where $\mathbf{C}, \mathbf{W}$ and $\mathbf{H}$ are sparse matrices. $\mathbf{C} \in \mathbb{R}^{m\times m}$ contains the convolution with I^{2D} at the focal point, $\mathbf{W} \in \mathbb{R}^{m\times n}$ is the X-ray forward projection and $\mathbf{H} \in \mathbb{R}^{n\times n}$ is the correction matrix. The reconstruction is computed iteratively by gradient descent. We further refer to this algorithm as THz-SIRT.

DART follows an iterative procedure of alternating 'updating' and 'discretisation' steps, with the latter using the prior knowledge of the gray levels [10]. The proposed DART-based THz reconstruction algorithm (THz-DART) follows a similar scheme and is presented in Fig. 1. Using THz-SIRT, an initial reconstruction of the phantom is computed (Fig. 2a-2b). This reconstruction is then segmented (Fig. 2c) to contain only the known gray levels of the object. Using a set of thresholds according to $\tau_i = \frac{\rho_i+\rho_{i+1}}{2}$ with the set of known gray levels: $R = \rho_1, \ldots, \rho_l$, the segmentation function becomes:

$$r(v) = \begin{cases} \rho_1 & (v < \tau_1) \\ \rho_2 & (\tau_1 \leq v \leq \tau_2) \\ & \vdots \\ \rho_l & (\tau_{l-1} \leq v) \end{cases} \tag{5}$$

From the segmented image, the set of boundary pixels is computed: pixels that do not have the same value as at least one of their 8-connected neighbours. These boundary pixels are taken into consideration in the next run of the THz-SIRT; all other pixels are fixed to their current value. However, if in the initial reconstruction parts of the object are not discerned due to having small boundaries, these will not be defined in the final reconstruction, as only the boundary pixels will update over time. To ensure that all parts of the object can be defined, a set of randomly chosen non-boundary pixels will also be updated by the algorithm, allowing for new boundaries to be created. In each THz-DART iteration, these pixels are chosen with a $1-P$ probability, with $0 < P < 1$ and together with the boundary pixels form the set of 'free pixels'. The other 'fixed pixels' are removed from the system of linear equations and their contribution to the sinogram p is removed. The number of equations in the system remains the same, but the amount of variables is reduced. Lowering the 'fix probability' P adds to the variables of the system, leading to a slower convergence as the projection error is spread out over more pixels.

After fixing one pixel x_i, the forward projection (Eq. 4) is transformed to [10]:

$$\mathbf{CW} \begin{pmatrix} \vdots & & \vdots & \vdots & & \vdots \\ h_1 & \cdots & h_{i-1} & h_{i+1} & \cdots & h_n \\ \vdots & & \vdots & \vdots & & \vdots \end{pmatrix} \begin{pmatrix} x_1 \\ \vdots \\ x_{i-1} \\ x_{i+1} \\ \vdots \\ x_n \end{pmatrix} = \mathbf{p} - v_i h_i \tag{6}$$

This is repeated for all fixed pixels. This new system is now solved by the THz-SIRT, for a set number of iterations referred to as (sub-DART). The new reconstruction combines the fixed pixels and the new values of the free pixels. As these free pixel values are not segmented, the reconstruction is segmented again to conclude the THz-DART iteration (Fig. 2e). An ending criterion must be given, as it is not ensured that the THz-DART converges to any value.

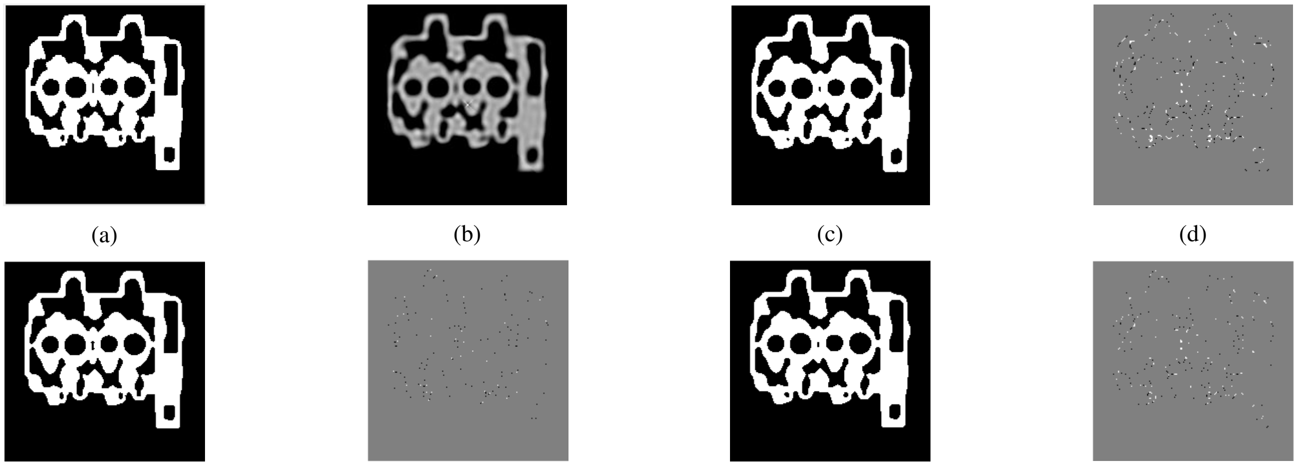

(a) (b) (c) (d)

(e) (f) (g) (h)

Figure 2: (a) The phantom, (b) initial THz-SIRT reconstruction at 1000 iterations, (c) segmented initial THz-SIRT reconstruction, (d) difference between the phantom and the initial reconstruction, (e) segmented THz DART reconstruction after 7000 SIRT iterations, (f) difference between the phantom and the THz-DART reconstruction, (g) segmented THz-SIRT reconstruction after 7000 iterations, (h) difference between the phantom and the segmented THz-SIRT reconstruction.

3 Experiments

Aside from the chosen beam properties, there are many other potential variables in the THz-DART experiments: the initial number of iterations, the fix probability p, the sub-DART iterations, the THz-DART iterations, the number of projections and the angular range. This section discusses various simulation experiments, examining the influence of these variables and comparing the results of THz-DART to the segmented THz-SIRT. The comparisons are made using the pixel-error of the (segmented) reconstructions (Fig. 2e-2h) and the number of iterations of the segmented THz-SIRT (the initial iterations + the total sub-DART iterations).

Simulation experiments were performed using binary phantoms (Fig. 2a, 5a), varying each of the examined variables in turn. The properties of the used beam are $\omega_0 = 3mm$ and $\lambda = 1mm$. Unless otherwise stated, the simulations are made with 200 initial iterations, $P = 1$, sub-DART= 10, 210 equi-angular projections and for a full angular range (0 to 180 degrees). A set amount of iterations was chosen as the ending criterion of THz-DART.

3.1 Initial iterations

The influence of the amount of iterations of the initial THz-SIRT reconstruction on the THz-DART reconstruction is examined comparing an initial reconstruction of 50 and 200 iterations (Fig. 3a, 3b). If there are few initial iterations, there will still be many incorrect non-boundary pixels in the THz-SIRT reconstruction. As THz-DART only changes the boundary pixels, compared to all pixels in the THz-SIRT, improvement of the THz-DART reconstructions will then be slower or similar to the ones of THz-SIRT (Fig. 4a). Especially for a low number of iterations of the reconstruction algorithm, THz-SIRT outperforms THz-DART. As the number of initial iterations increases, the bulk of the object will be sufficiently well reconstructed; most incorrect pixels in the reconstruction will be boundary pixels, providing a significant advantage to THz-DART (Fig. 4b). A sufficient number of initial iterations is necessary for the THz-DART to perform efficiently, this number is dependent on the complexity of the object. All further simulations are made with 200 or more initial iterations.

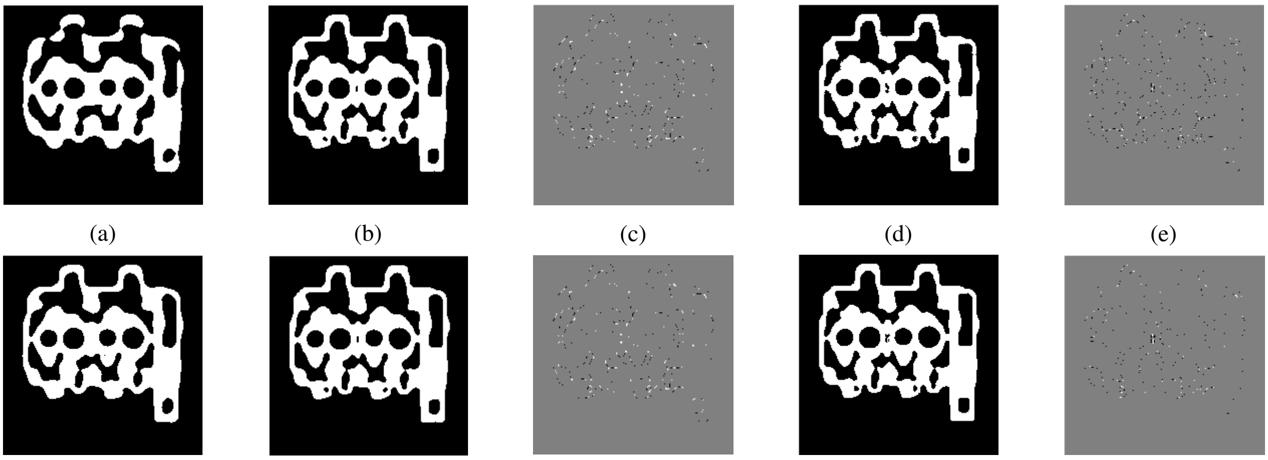

(a) (b) (c) (d) (e)

(f) (g) (h) (i) (j)

Figure 3: (a, f) Initial segmented THz-SIRT reconstruction, (b,g) segmented THz-SIRT reconstruction after 2000 iterations, (c, h) its residual image, (d, i) THz-DART reconstruction after 2000 iterations, and its residual image at (e) 50 and (j) 200 initial iterations.

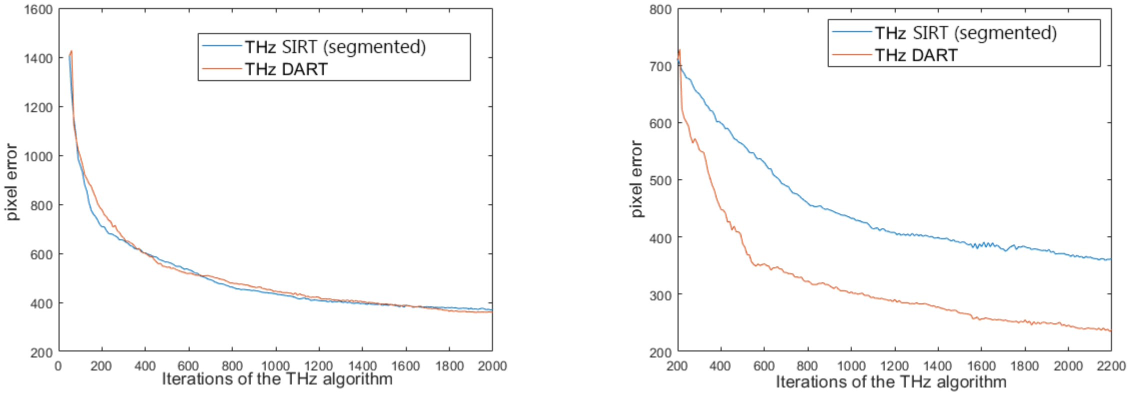

(a) (b)

Figure 4: Pixel error of the segmented THz-SIRT and the THz-DART reconstruction for (a) 50 and (b) 200 initial iterations.

3.2 Fix probability

The fix probability P determines the amount of free non-boundary pixels. For an object with small inner boundaries (Fig. 5a), the initial reconstruction (Fig. 5b) does not capture these parts of the object. For $P = 1$, the edges of the THz-DART reconstruction (Fig. 5c) are much improved but the hole of the object is not discerned as no new boundaries are created. With $P = 0.7$ however, the hole in the object has become visible, and the definition of the edges of the object are improved (Fig. 5d). In the equivalent segmented THz-SIRT reconstruction (Fig. 5e), the hole in the object is not discerned. As the hole is small compared to the bulk of the object, the projection error is also small when it is not discerned. In THz-SIRT, the projection error is divided over all pixels. A small projection error will lead to small changes in the pixel values of the reconstruction. This in turn will reduce the chance that a pixel will pass the threshold value of the segmentation function. As a result, segmented THz-SIRT is not capable of discerning small object structures.

In 6a, the pixel error of the THz-DART reconstructions for various P-values and the segmented THz-SIRT reconstructions is given. Although the small hole of the object will not be discerned in the THz-DART reconstruction for $P = 1$, the quality of the reconstruction is much better than that for other P values. As the object has a mostly homogeneous structure, most improvements can be made at the outer edges of the object. Without the extra free pixels, i.e. $P = 1$, the reconstruction can thus converge faster to a lower pixel error, although it will never reach the ground truth. All THz-DART reconstructions outperformed the segmented THz-SIRT reconstructions.

3.3 Number of projections

The number of projections, i.e. the number of measurements, is an important variable to examine as THz measurements are slow - a known drawback in THz imaging. The comparison of the THz-DART and segmented THz-SIRT reconstructions after 7000

(a) (b) (c) (d) (e)

Figure 5: (a) The phantom, (b) segmented THz-SIRT reconstruction at 200 iterations, (c) THz-DART reconstruction for $P = 1$ after 500 iterations, (d) THz-DART reconstruction for $P = 0.7$ after 500 iterations, (e) segmented THz-SIRT reconstruction after 500 iterations.

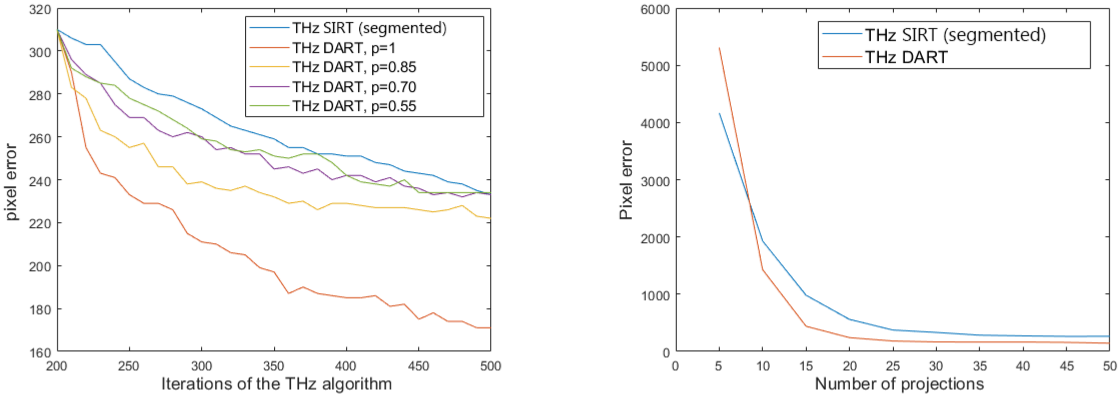

(a) (b)

Figure 6: Pixel error of the segmented THz-SIRT and THz-DART reconstructions (a) for various P-values, (b) as a function of number of projections.

iterations are given in Fig. 6b. For an extremely low number of projections (<10), the initial reconstruction contains too many artefacts to ensure that the THz-DART reconstruction recovers from only updating the boundary pixels.

For a sufficiently large number of projections (>10), the initial reconstruction is accurate enough to ensure a well defined problem for the THz-DART. Although the THz-DART reconstruction now has a lower pixel error, after a certain amount of projections ($\sim$ 30) improvement in both reconstructions stagnates. The projection error is divided over all pixels in the segmented THz-SIRT. As the projection error decreases, so do the changes in the pixel values of the reconstruction, which reduce the chances of the pixel changing its value after being segmented. This also occurs for THz-DART as one iteration of the THz-DART incorporates a set amount of iterations (sub-DART) of the segmented THz-SIRT. Although the projection error will only be divided over the boundary pixels, the algorithm is limited to fewer iterations before the segmentation.

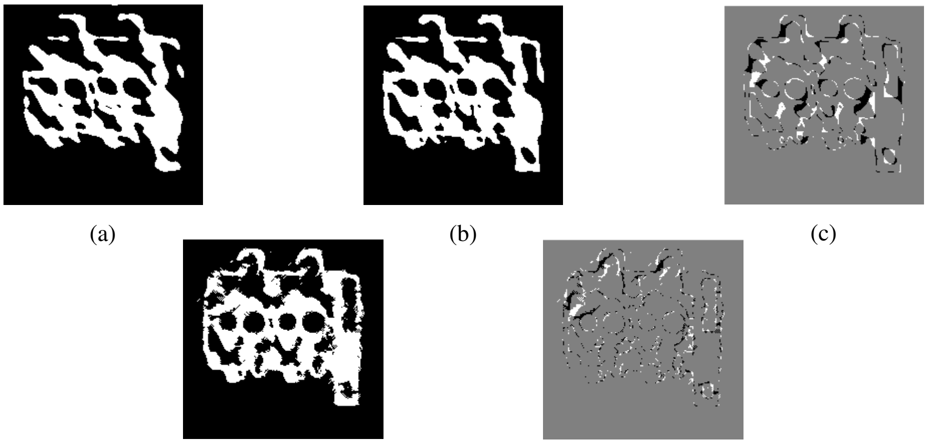

(a) (b) (c)

(d) (e)

Figure 7: For 80 degrees angular range: (a) the initial segmented THz-SIRT reconstruction at 1000 iterations, (b) segmented THz-SIRT reconstruction at 7000 THz iterations, (c) difference between the phantom and the segmented THz-SIRT reconstruction, (d) THz-DART reconstruction, (e) Difference between the phantom and the THz-DART reconstruction.

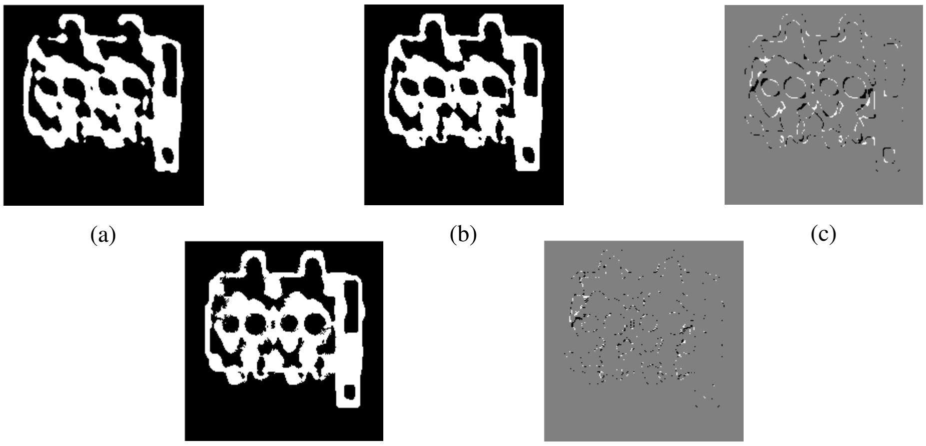

(a) (b) (c)

(d) (e)

Figure 8: For 100 degrees angular range: (a) initial segmented THz-SIRT reconstruction at 1000 iterations, (b) segmented THz-SIRT reconstruction at 7000 iterations, (c) difference between the phantom and the segmented THz-SIRT reconstruction, (d) THz-DART reconstruction, (e) difference between the phantom and the THz-DART reconstruction.

3.4 Limited angular range

In limited angle simulations, there is a ’missing wedge’ in the angular projection range. These experiments examine the influence of a varying missing wedge (steps of 10 degrees), using the same amount of projections for each simulation. The initial reconstruction is made with 1000 iterations and the reconstructions are made with sub-DART= 20 iterations. Fig. 7 and 8 show the initial and final segmented THz-SIRT and THz-DART reconstructions after 11000 SIRT iterations at 80 and 100 degrees angular range respectively. The pixel errors of these reconstructions are given in Fig. 9a and 9b. A comparison of the final reconstructions in function of the angular range is given in Fig. 9c.

If the missing wedge is larger than 120 degrees, the problem is badly defined and, similar to the previous simulations, the segmented THz-SIRT performs better. Although the THz-DART reconstruction has a higher pixel error, it contains less smearing than the segmented THz-SIRT. After 60 degrees angular range, THz-DART provides a better reconstruction. While the reconstructions of both algorithms improve with increasing angular range, improvement stagnates at large angular ranges without reaching the ground truth solution, following the observations of the previous simulations.

4 Discussion

The simulations demonstrated the advantage of THz-DART in terms of reconstruction quality and convergence rate, compared to segmented THz-SIRT. However, THz-DART depends on a number of settings that have to be (heuristically) set, such as the number of iterations as well as the update probability, both which may influence the resulting reconstruction quality. Furthermore, accurate knowledge of the object’s gray levels is assumed. In case the grey levels are unknown (i.e., if only the *number* of grey levels is known), they need to be estimated during the reconstruction. This has been demonstrated for DART (cfr. [11]) but has yet to be developed for THz-DART. Finally, future work will also include simulations on phantoms with more than two gray levels and will include real data experiments.

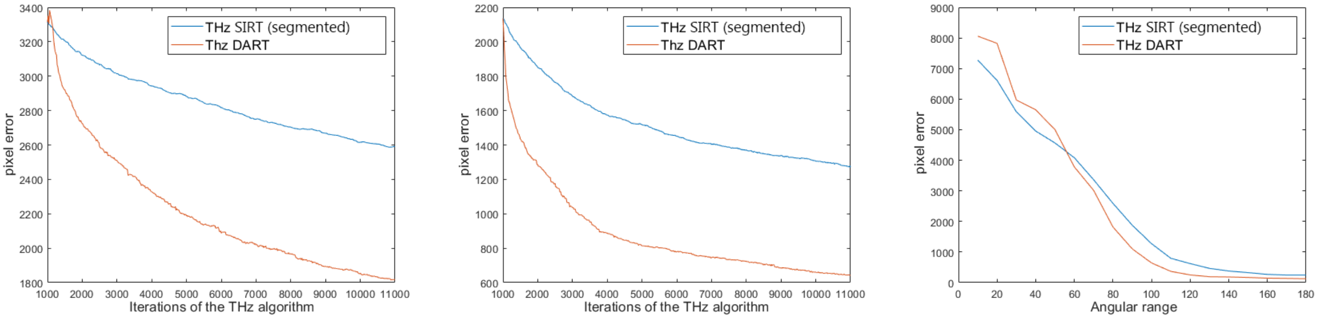

(a) (b) (c)

Figure 9: Pixel error comparison of the THz-DART and segmented THz-SIRT reconstructions for (a) 80 degrees angular range, (b) 100 degrees angular range, (c) as a function of the angular range in final reconstructions.

5 Conclusion

In this paper, a reconstruction algorithm for discrete THz tomography that incorporates the THz beam shape was presented. Simulation experiments showed that THz-DART consistently converges faster and yields images with higher reconstruction quality compared to the one from segmented THz-SIRT.

Acknowledgements
This work was financially supported by FWO Flanders (Grant No. 1SD9621N and S004217N).

References

[1] Ellrich, F. et al., "Terahertz Quality Inspection for Automotive and Aviation Industries, Journal of Infrared, Millimeter, and Terahertz Waves", 41(4) (2019), 470-489.
[2] Zimdars, D. et al., "Time Domain Terahertz Imaging Of Threats In Luggage And Personnel", International Journal of High Speed Electronics and Systems, 17(02) (2007), 271-281.
[3] Bessou, M., Chassagne, B., Caumes, J., et al., "Three-dimensional terahertz computed tomography of human bones", Applied Optics, 51(28) (2012), 6738-6744
[4] Jackson, J. B. et al., "A Survey of Terahertz Applications in Cultural Heritage Conservation Science", IEEE Transactions on Terahertz Science and Technology, 1(1) (2011), 220-231.
[5] Recur, B., et al., Investigation on reconstruction methods applied to 3D terahertz computed tomography, Optics Express, 19(6) (2011), 5105-5117
[6] B. Recur, J.P. Guillet, I. Manek-Hönninger, et al., “Propagation beam consideration for 3D THz computed tomography”, Optics Express, 20(5) (2012), pp. 5817–5829
[7] P. Paramonov, Lumbeeck, L. - P., De Beenhouwer, J., and Sijbers, J., “Accurate terahertz simulation with ray tracing incorporating beam shape and refraction”, in IEEE ICIP, pp. 3035-3039, 2020
[8] A. Duhant, M. Triki, and O. Strauss, “Terahertz differential computed tomography: a relevant nondestructive inspection application”, Journal of Infrared, Millimeter,and Terahertz Waves, 40 (2019), 178–199
[9] L.P. Lumbeeck, P. Paramonov, J. Sijbers, J. De Beenhouwer, "The Radon transform for Terahertz computed tomography incorporating the beam shape", in IEEE ICIP, pp. 3040-3044, (2020)
[10] K.J. Batenburg, J. Sijbers, "DART: A practical reconstruction algorithm for discrete tomography", IEEE Transactions on Image Processing, 20(9) (2011), 2542-2553.
[11] W. Van Aarle, Batenburg, K. J., and Sijbers, J., “Automatic parameter estimation for the Discrete Algebraic Reconstruction Technique (DART)”, IEEE Transactions on Image Processing, vol. 21, no. 11, pp. 4608-4621, 2012